Understanding shape entropy through local dense packing: Supplementary Information

Greg van Anders [*], **Daphne Klotsa** [*], **N. Khalid Ahmed** [*], **Michael Engel** [*], **Sharon C. Glotzer** [*] [†]

[*]Department of Chemical Engineering, University of Michigan, Ann Arbor, MI 48109-2136, USA, and [†]Department of Materials Science and Engineering, University of Michigan, Ann Arbor, MI 48109-2136, USA

Supplementary Methods

Further Analytical Considerations.

Jacobian Factor

We have included the Jacobian factor in our definition of the PMFT. The motivation for doing this is that by explicitly including this term we do not want to either ignore or introduce any artifacts that might stem from a poor choice of coordinates for a given problem. Note that for general particles in three dimensions, the PMFT is defined on the space $\mathbb{R}^3 \times \mathbb{RP}^3$. This means that even if the pair interaction is purely hard, whenever there is non-trivial shape, some relative pair configurations are preferred over others. In standard treatments of the isotropic potential of mean force, it is not conventional to include the Jacobian factor. The choice not to include it in that case is well-motivated by the existence of a single "natural" coordinate system in that case that prevents any ambiguity there. In either case, one must take account of the inclusion or not of this factor in writing down the effective equations of motion for the pair.

Axisymmetric Coordinate System for PMFT

We present an explicit computation of the Jacobian of the change of variables between the natural coordinates of a pair of particles, and the scalar invariant quantities that describe any such pair. We do so in the simpler case of axisymmetric particles. The general case can be computed straightforwardly in the same manner, but the expressions are cumbersome.

We take the first particle to be at the origin, with its symmetry axis oriented in the positive z direction. Using the azimuthal symmetry with this placement, we fix the second particle's position in the xy-plane, without loss of generality to be along the x axis. This gives the orientation of the second particle as

$$\hat{n}_2 = \sin\theta\cos\varphi\hat{x} + \sin\theta\sin\varphi\hat{y} + \cos\theta\hat{z} \qquad [1]$$

where θ and φ are spherical coordinates in the coordinate system of the second particle, and its position as

$$r_2 - r_1 = \rho\hat{x} + z\hat{z} \qquad [2]$$

where ρ and z are cylindrical coordinates in the first particle's coordinate system. The volume form that appears in the integral that computes the partition function is

$$dV = \rho\sin\theta d\rho dz d\theta d\varphi \qquad [3]$$

Now we make the change of variables to the scalar invariant quantities by taking

$$\begin{aligned} R &= \sqrt{z^2+\rho^2} \\ \phi_1 &= \frac{z}{\sqrt{z^2+\rho^2}} \\ \phi_2 &= -\frac{\rho\sin\theta\cos\varphi + z\cos\theta}{\sqrt{z^2+\rho^2}} \\ \chi &= -\cos\theta \end{aligned} \qquad [4]$$

Inverting the relationship between the two coordinate systems gives

$$\begin{aligned} \rho &= R\sqrt{1-\phi_1^2} \\ z &= R\phi_1 \\ \theta &= -\cos^{-1}\chi \\ \varphi &= \cos^{-1}\left(\frac{-\phi_1\chi - \phi_2}{\sqrt{(1-\chi^2)(1-\phi_1^2)}}\right) \end{aligned} \qquad [5]$$

The computation of the determinant is simplified by noting the dependence of ρ and z on only R and ϕ_1, and θ on only χ. This means that we only need to consider the dependence of φ on ϕ_2. Taking the determinant of this leads to the new volume form

$$dV = \frac{R^2 dR d\phi_1 d\phi_2 d\chi}{\sqrt{1-\chi^2-\phi_1^2-\phi_2^2-2\phi_1\phi_2\chi}} \qquad [6]$$

In the absence of the excluded volume (or other) interaction between the particles, this expression measures the volume of configuration space available to a pair of free particles in a particular translationally and rotationally invariant configuration.

To verify that our expression correctly encodes the density of states for two free axisymmetric particles, we consider the following scenario. Suppose we had a pair of axisymmetric particles each undergoing Brownian motion with the constraint that their centers of mass could never be separated by a distance greater than R_{max}, but that they were otherwise free to move, including to interpenetrate. If we were to make some N_{obs} uncorrelated observations of the particles for each of which we determine the values of R, ϕ_1, ϕ_2, and χ, we would find that their frequency distribution would converge to something proportional to the Jacobian of our coordinate transformation in the limit that $N_{\text{obs}} \to \infty$. We therefore verified our expression by performing precisely this calculation.

General Coordinate System for PMFT

For the general case in three dimensions, a pair of particle has six degrees of freedom that are invariant under global translations and rotations. Let us take the particles to be situated at $\vec{r}_{1,2}$, and have orientations $\mathbf{q}_{1,2}$. Starting with the positions, the separation of the particles in position space is simply given by the vector $\vec{r}_{12} = \vec{x}_2 - \vec{x}_1$. This gives a set of coordinates that are invariant under translations, but not under rotations. We therefore seek to form six scalars by taking combinations of this vector with the particle orientations.

To treat the particle orientations on a similar footing to the positions, we need to determine the separation in orientation of the particles. We note that that each of the particle orientations is given by an element of $SO(3)$, the rotation group in three dimensions. While it is possible to work with this group directly, the calculations that follow can be simplified greatly by noting that $SU(2)$ is the double cover of $SO(3)$, and working with $SU(2)$ instead. For concreteness, we will use the conventions common in quantum mechanics and write our particle orientations as rotation operators according to

$$\mathbf{q}_i = e^{i\frac{\theta_i}{2}\hat{n}\cdot\vec{\sigma}}\,, \qquad [7]$$

where θ_i is the angle of rotation $\hat{n}_i$ is the normal to the plane of the rotation and $\vec{\sigma}$ are the Pauli matrices. From this form it is clear that

under a global rotation, the particle orientations transform in the reducible representation expressed in Young tableaux as

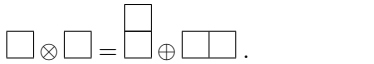

[8]

This can be understood intuitively in the following way: if you rotate a particle by some amount in some plane, two different observers will agree on the amount of the rotation, but will give the normal to the plane in their own coordinates. The amount of the rotation is the scalar  , and the normal to the plane is the vector  . In a similar fashion to the way in which we combined particle positions to yield a relative position, we will combine particle orientations. A Clebsh-Gordan decomposition of the particle orientations gives

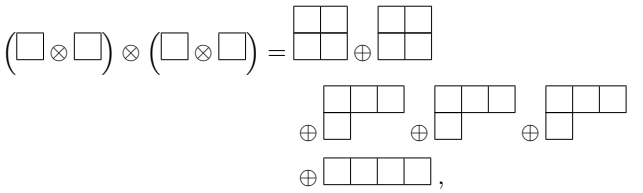

[9]

which means that the combination of the two orientations yields two scalars (spin 0), three vectors (spin 1), and a tensor (spin 2).

For convenience, we note that the spin 1 representation of $SU(2)$  is also the adjoint representation of $SU(2)$. This means that we can write vectors in ordinary space by using the Pauli matrices as Cartesian unit vectors according to

$$\vec{v} = \sum_i \vec{v} \cdot \hat{e}_i \sigma_i \ . \tag{10}$$

In this representation, if we combine orientations expressed in terms of Pauli matrices as in **[7]**, products of orientations that are proportional to the identity matrix are scalar quantities, and products that are not are vectors. We will use this fact momentarily.

For the purposes of creating scalar invariants by combining them among themselves, and with the particle separation in position, the scalars and vectors that arise from combining orientations are of interest. We determine these scalars and vectors explicitly by taking symmetrized Hermitian products of the particle orientations. We find the scalars can be expressed as

$$\begin{aligned} S_{12} =& \frac{1}{2}(\mathbf{q}_1\mathbf{q}_2^\dagger + \mathbf{q}_2\mathbf{q}_1^\dagger) \\ U_{12} =& \frac{1}{4}(\mathbf{q}_1\mathbf{q}_2 + \mathbf{q}_2\mathbf{q}_1 + \mathbf{q}_1^\dagger\mathbf{q}_2^\dagger + \mathbf{q}_2^\dagger\mathbf{q}_1^\dagger) \end{aligned} \tag{11}$$

and the vectors as

$$\begin{aligned} V_{12} =& \frac{i}{4}(\mathbf{q}_1\mathbf{q}_2 - \mathbf{q}_2\mathbf{q}_1 + \mathbf{q}_1^\dagger\mathbf{q}_2^\dagger - \mathbf{q}_2^\dagger\mathbf{q}_1^\dagger) \\ W_{12} =& -\frac{i}{4}(\mathbf{q}_1\mathbf{q}_2 + \mathbf{q}_2\mathbf{q}_1 - \mathbf{q}_1^\dagger\mathbf{q}_2^\dagger - \mathbf{q}_2^\dagger\mathbf{q}_1^\dagger) \\ T_{12} =& -\frac{i}{2}(\mathbf{q}_1\mathbf{q}_2^\dagger - \mathbf{q}_2\mathbf{q}_1^\dagger) - V_{12} \end{aligned} \tag{12}$$

which we have identified according to their matrix form. Using our convention for representing the particle orientations we find

$$\begin{aligned} S_{12} =& \cos\left(\frac{\theta_1 - \theta_2}{2}\right) \\ U_{12} =& \cos\left(\frac{\theta_1 + \theta_2}{2}\right) \\ V_{12} =& \frac{1}{2}(\hat{n}_1 \times \hat{n}_2)(S_{12} - U_{12}) \\ W_{12} =& \sin\left(\frac{\theta_1 + \theta_2}{2}\right)\frac{\hat{n}_1 + \hat{n}_2}{2} + \sin\left(\frac{\theta_1 - \theta_2}{2}\right)\frac{\hat{n}_1 - \hat{n}_2}{2} \\ T_{12} =& \sin\left(\frac{\theta_1 + \theta_2}{2}\right)\frac{\hat{n}_1 + \hat{n}_2}{2} - \sin\left(\frac{\theta_1 - \theta_2}{2}\right)\frac{\hat{n}_1 - \hat{n}_2}{2} \end{aligned} \tag{13}$$

By combining these quantities with $\vec{r}_{12}$ we can form the six scalar invariants

$$\{|\vec{r}_{12}|,\ S_{12},\ U_{12},\ \hat{r}_{12}\cdot W_{12},\ \hat{r}_{12}\cdot V_{12},\ W_{12}\cdot T_{12}\} \tag{14}$$

For the purposes of showing the coordination of particles in space at the location of faces or facets, it is convenient to integrate over some of the angular degrees of freedom, and to work in Cartesian coordinates. In particular, it is very convenient to work in Cartesian coordinates adapted to the particle facets as shown in Fig. 1 for tetrahedral facets.

Forces and Torques

For concreteness, we give an example for how to compute the forces and torques from the PMFT. As usual, forces and torques arise from taking the negative gradient of the potential. For force components this is straightfoward. For torques, we give an explicit expression for the case of axisymmetric particles.

To compute the torques, we continue to work in terms of rotation matrices in the spin $\frac{1}{2}$ representation of $SU(2)$. If $\mathbf{q}$ is the rotation, then to determine the torque, we must differentiate the PMFT with respect to it. If we represent the rotations in the canonical fashion, and use Pauli matrices as the basis vectors of the Cartesian space coordinates, then we have scalar products of the form

$$\vec{a}\cdot\vec{b} = \frac{1}{2}\,\mathrm{Tr}(a^\dagger b) \tag{15}$$

and cross products of the form

$$\vec{a}\times\vec{b} = \frac{1}{2i}[a,b] \tag{16}$$

Our potential depends on scalar products alone. That means to determine the torque we are required to know, *e.g.*, that if

$$\phi_1 = \frac{1}{2}\,\mathrm{Tr}(\mathbf{q}^\dagger\hat{z}\mathbf{q}\hat{r}_{12}) \tag{17}$$

then

$$\frac{\partial\phi_1}{\partial\mathbf{q}} = \frac{1}{2}\mathbf{q}^\dagger\left[\mathbf{q}\hat{r}_{12}\mathbf{q}^\dagger, \hat{z}\right] \tag{18}$$

which we recognize as a cross product. We have taken, without loss of generality, the reference vector to be $\hat{z}$ in the coordinate frame of the particle. We then use the chain rule to differentiate F_{12} with respect to $\mathbf{q}$, and convert back to Cartesian coordinates to find a contribution to the torque of the form

$$\vec{T}_{\phi_1} = -\hat{r}_{12}\times\hat{n}_1\frac{\partial F_{12}}{\partial\phi_1} \tag{19}$$

Similar manipulations yield the other contributions.

Numerical Methods.

Monodisperse Systems

For hard particle systems, the various contributions in Eq. (5) (main text) can be computed using different means. The pair interaction term (βU) is given by the pair overlap function, which is known, at least in principle. The pair Jacobian term ($-\log J$) can be computed analytically, as we describe below. The third contribution ($\beta\tilde{F}_{12}$) could be computed by determining the free energy of the rest of the system for a series of fixed configurations of the pair. In practice, we are not interested in the contributions of each of the individual terms *per se*, so instead we compute their sum directly. We obtain the PMFT on the left hand side of Eq. (5) (main text) by computing the frequency histogram of the relative pair coordinates and orientations, and taking its logarithm, as suggested by the form of Eq. (4) (main text). This gives the PMFT up to an overall irrelevant additive constant[1].

Since the PMFT is a generalization of the potential of mean force, the method for computing the PMFT is a straightforward generalization of the method used to extract the potential of mean force from the radial distribution function $g(r)$. In detail, over the course of a MC simulation trajectory, we measure all of the relative positions of each pair of particles that fall within a given cutoff distance (for the results we present in the main text we integrate over the relative orientations). We impose a discrete grid over the set of allowed relative positions, and record the number of pairs that fall within each grid cell. This tabulation of the relative frequency of the various configurations, gives us a measurement of the $g(x,y,z)$ analogue of $g(r)$, and so simply taking the logarithm gives us F_{12} from Eq. (5) (main text).

Computing the PMFT in this manner introduces two forms of systematic discretization error. To illustrate the sources of this error we will give a more detailed description of the calculation we performed. We wish to compute the PMFT at some given relative position and orientation. For concreteness, and to keep formulae simple, let us consider just computing the force component. In principle, one can compute the PMFT by performing thermodynamic integration or umbrella sampling over various fixed relative particle positions if one wants the exact potential difference between particular relative pair positions and orientations. However, in our case we are interested in the general geometric features of the potential, for which it is sufficient to perform simulations in a standard ensemble, and record the relative frequency of various events. Thus we compute an approximate value, F'_{12}, of the true PMFT, F_{12}, at some point (x_i, y_i, z_i) by averaging over a bin of size $(\Delta x, \Delta y, \Delta z)$ centered at that point according to

$$\Delta x\Delta y\Delta z e^{-\beta F'_{12}(x_i,y_i,z_i)} \equiv \int_{\text{bin}_i} dxdydz e^{-\beta F_{12}(x,y,z)} \ . \quad \textbf{[20]}$$

If the true potential of mean force and torque is slowly varying over the bin, in the sense that

$$\left| \int_{\text{bin}_i} dxdydz(\vec{x}-\vec{x}_i)\cdot\nabla\ e^{-\beta F_{12}(x,y,z)}\Big|_{\vec{x}=\vec{x}_i} \right| \ll \Delta x\Delta y\Delta z e^{-\beta F_{12}(x_i,y_i,z_i)} \ , \quad \textbf{[21]}$$

then we can Taylor expand the integrand about (x_i, y_i, z_i), and, assuming that the whole bin is allowed, we find that

$$\Delta x\Delta y\Delta z e^{-\beta F'_{12}(x_i,y_i,z_i)} \approx \Delta x\Delta y\Delta z e^{-\beta F_{12}(x_i,y_i,z_i)} \ . \quad \textbf{[22]}$$

This gives $F'_{12}(x_i,y_i,z_i) \approx F_{12}(x_i,y_i,z_i)$. This approximation breaks down if F_{12} is not sufficiently slowly varying, in the above sense. It also breaks down if the bin is partially forbidden, *i.e.* if the integrating volume is not $\Delta x\Delta y\Delta z$. We expect the PMFT to vary quickly at the boundaries of regions that are forbidden due to overlap, *i.e.* we expect the effective potential to be relatively "hard". This means that at the edges of these regions, where we would have difficulty sampling events, we would also expect to have to resolve minute differences to obtain meaningful results. This makes such a technique prohibitively difficult for such boundary cases where one would have to resort to umbrella sampling. As a result (in particular in Figs. 2, 3, and 5, main text) we only show the PMFT for points that are within 4 $k_{\text{B}}T$ of the global minimum, because it is at these points that we can sample the potential reliably in the sense described above, using our method.

Penetrable Hard Sphere Systems

Here we explain how we calculate the PMFT for a pair of hard, arbitrarily shaped colloidal particles in a sea of smaller penetrable hard sphere depletants.

As we showed in Eq. (9) (main text), the PMFT takes on a simplified form in the case of penetrable hard sphere depletants and thus the contribution from integrating out the depletants $\tilde{F}_{12}$ can be computed more easily. The contribution from the colloid pair potential is, in principle, known, as before, and the Jacobian can be computed as described below. The problem is therefore reduced to computing the contribution that comes from the free volume available to the depletants for a fixed configuration of the colloidal pair.

We computed the free volume in the penetrable hard sphere model of depletants by MC integration. The same results could also be obtained by direct MC simulations with explicit ideal depletants, as discussed below, or by some other numerical integration method. To accelerate this computation, we make note of the following. The change in free volume between a given configuration and widely separated particles falls entirely within the intersection of two spheres, each enclosing a particle. The volume of this region of intersection is smallest (and, therefore, computation is most efficient) if the radii of the spheres in question are as small as possible. This is given by having a sphere enclosing each particle with a radius given by the sum of the radius of a sphere that circumscribes the particle and the radius of a sphere that circumscribes the depletant.

For a given relative position and orientation of the colloids, we computed the intersection of spheres that determined this region and computed the change in free volume by throwing random depletants uniformly over the region and computing the fraction that intersected both colloids. We performed five independent runs for each system. We used 500 MC integration points per unit volume of the region of intersection, and 1000 total throws if the volume of intersection was less than one unit. This fraction of the total volume gives the change in free volume available to the depletants. In the case of faceted spheres, overlap checks between particles were performed by casting the overlap as an optimization problem that we solved using the Karush-Kuhn-Tucker method [1]. In the case of spherocylinders, the Bullet physics library [2] was used to check overlaps.

As noted above, the Jacobian of the transformation to invariant coordinates can be computed analytically, which we did. We checked our analytical calculation numerically by performing a MC simulation of a pair of free axisymmetric particles. The frequency histogram of the occurrence of the invariant coordinates was checked against the analytic form and found to match.

To examine these systems in detail it is convenient to use the language of entropic patches from [3]. We define the probability of specific binding at a pair of entropic patch sites as the probability of finding a pair of particles at the set of configurations that are in the basin of attraction of perfect alignment. We obtain this by integrating the Boltzmann weight over the set of configurations.

[1] Because the PMFT is a potential, only differences in the PMFT between points are meaningful; it's value is not. Potential differences are not affected by shifting the potential by a constant everywhere, so one can only ever compute the potential up to a constant shift.

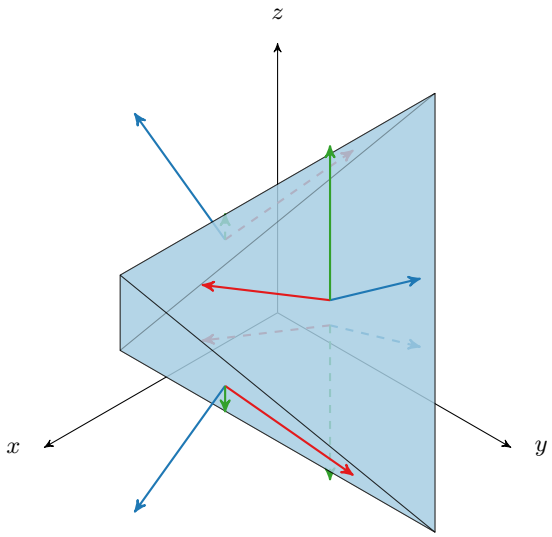

Fig. 1. An illustration of the choice of four sets of orthogonal coordinates for each of the faces of a tetrahedron, which we use for subsequent computations in Figs. 2 and 3 (main text). The face normals, which we take to be the z coordinates in the frame of the face are shown in blue. Similarly, the x and y coordinates in the frame of the face are shown in green and red respectively.

For concreteness, consider a pair of hemispherical particles in a bath of depletants. The probability of specific binding can be cast formally as the integral

$$Z_s \propto \int_0^1 d\phi_1 \int_0^1 d\phi_2 \int dR d\chi e^{-\beta F_{12}(R,\phi_1,\phi_2,\chi)} H(-\beta P \Delta V_{\rm F}) \ . \quad [23]$$

The upper bounds on the ϕ integrals correspond to coincident faces. The step H function ensures that we are only integrating over configurations in which there is entropic binding. Similar integrals can be defined for semi-specific binding (patch to non-patch) and non-specific binding (non-patch to non-patch).

Comparison of Methods for Penetrable Hard Sphere Depletants

The results we obtained via free volume calculations with ideal depletants can also be obtained via simulations with explicit depletants. To see why the two forms of computation are equivalent, we consider the following situation. Again, for the sake of simplicity, we will work in the penetrable hard sphere limit. The probability of accepting a trial Monte Carlo move of our colloidal particle is given by

$$p_a = (1-p)^N \quad [24]$$

where N is the number of depletants, and p is the probability that a depletant will be in the region swept out by the particle during its move. In the limit in which we are working, this is given by

$$p = \frac{\Delta V_{\rm sweep} - \Delta V_{\rm overlap}}{V_{\rm F}} \quad [25]$$

where $V_{\rm F}$ is the free volume available to the depletants, $\Delta V_{\rm sweep}$ is the volume swept out by the colloid during move, and $\Delta V_{\rm overlap}$ accounts for any increase in the depletant overlap volume.

In the limit that the move is small, *i.e.* $Np \ll 1$, the probability of accepting the move is

$$p_a \approx 1 - \frac{N(\Delta V_{\rm sweep} - \Delta V_{\rm overlap})}{V_{\rm F}} \quad [26]$$

which gives the probability of rejecting such a move as

$$p_r \approx \frac{N(\Delta V_{\rm sweep} - \Delta V_{\rm overlap})}{V_{\rm F}} \quad [27]$$

We can, similarly, find the probability of rejecting a reverse move. That is given by

$$p_r' \approx \frac{N(\Delta V_{\rm sweep})}{V_{\rm F} + \Delta V_{\rm overlap}} \approx \frac{N \Delta V_{\rm sweep}}{V_{\rm F}} \left(1 - \frac{\Delta V_{\rm overlap}}{V_{\rm F}}\right) \quad [28]$$

where we have assumed that, without loss of generality, the "forward" move causes an increase in the depletant overlap volume, and the reverse move causes it to decrease. We have again also used the fact that the size of the move is small.

We compute the difference in probability for the two moves

$$\Delta p \equiv p_r' - p_r \approx \frac{N \Delta V_{\rm overlap}}{V_{\rm F}} \left(1 - \frac{\Delta V_{\rm sweep}}{V_{\rm F}}\right) \approx \frac{N \Delta V_{\rm overlap}}{V_{\rm F}} \ . \quad [29]$$

We can now consider another pair of moves in which the initial configuration of the forward move is identical to the situation just described, but the final configuration is different. If in that case the change in overlap volume is $\Delta V'_{\rm overlap}$, then the probability difference is

$$\Delta p' \approx \frac{N \Delta V'_{\rm overlap}}{V_{\rm F}} \quad [30]$$

From these quantities we can compute the ratio $\Delta p / \Delta p'$, which is dependent only on the free volume, which, in turn, is encoded in our potential of mean force and torque. We get that

$$\frac{\Delta p}{\Delta p'} = \frac{\Delta V_{\rm overlap}}{\Delta V'_{\rm overlap}} \quad [31]$$

which means we can write

$$\frac{\Delta p}{\Delta p'} = \frac{F_{12}^{\rm post} - F_{12}^{\rm pre}}{F_{12}^{\rm post\prime} - F_{12}^{\rm pre}} \quad [32]$$

in the limit that $T \to 0$. From this expression we see that the PMFT we deduced from the free volume calculation is precisely the quantity that controls the average acceptance rate of MC moves of the colloids in a simulation with explicit depletants. Hence results obtained from the free volume methods used above will precisely match those obtained using much more expensive MC simulations with explicit ideal depletants.

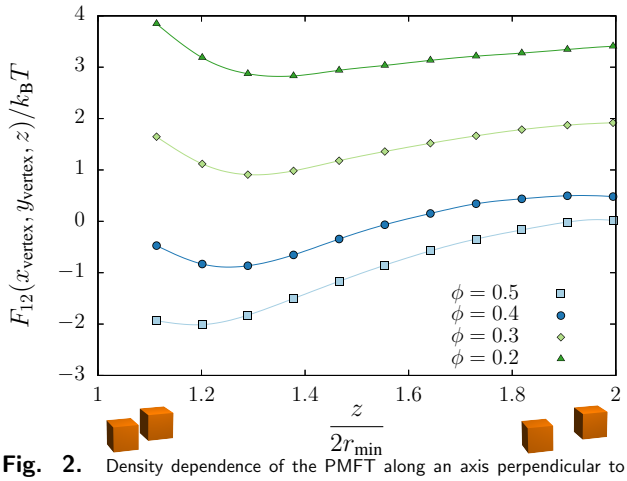

Fig. 2. Density dependence of the PMFT along an axis perpendicular to the polyhedral face for a hard cube fluid that passes through the cube vertex. Note that the expected increase in effective attraction that occurs as system density increases is less pronounced than the corresponding plot in Fig. 2c (main text) for an axis that passes through the center of the face.

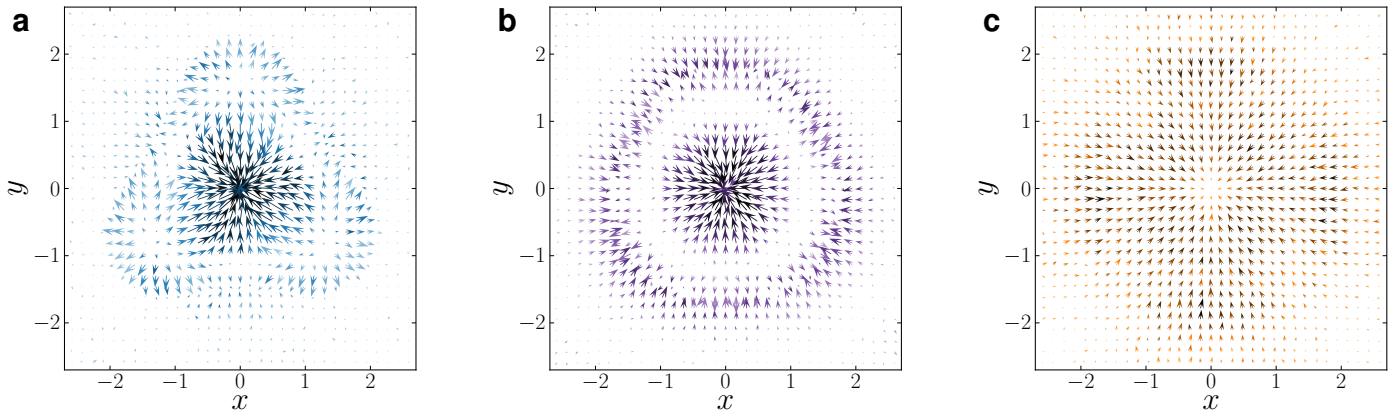

Fig. 3. DEFs in Cartesian coordinates for monodisperse hard particle systems at a packing fraction of $\eta = 0.4$ for tetrahedra (a), tetrahedrally facetted spheres (b), and cubes (c). DEFs are computed by approximating the negative gradient of the PMFT with finite differences. All cases show preference for face-to-face alignment, but as in Fig. 3 (main text) the strength of preference, and the shape of the forces, depends on particle shape.

Table S1. Angular dependence of PMFT for Hard Hemispheres

	$\psi \approx 0.95$	$\psi \approx 0.98$
		
$F_{12}(R=0.3)/k_{\mathrm{B}}T$	3.48 ± 0.05	1.16 ± 0.01
$F_{12}(R=0.4)/k_{\mathrm{B}}T$	3.64 ± 0.06	2.39 ± 0.03

Supplementary Results

Entropic Forces In Monodisperse Hard Systems. To capture DEFs, in the manuscript we computed the PMFT. Because the PMFT is a potential, forces are the negative gradient of it. For completeness in Fig. 3, we give explicit calculations of the DEFs for monodisperse hard systems in Cartesian coordinates in three example systems at a packing fraction of $\eta = 0.4$: tetrahedra (a), tetrahedrally facetted spheres (b), and cubes (c). The forces are computed using from the PMFT by approximating the gradient using finite differences. We show the force components in the plane of the facet. To produce the plots we have chosen to represent energies in units of length so that arrows are visible on the plots. From Fig. 3 (main text) it is can immediately be seen that overall scale of forces is on the order of $k_{\mathrm{B}}T/\sigma$ where σ is the relevant length scale for the particle. Panel (a) corresponds to Fig. 3c (main text), and shows that at $\eta = 0.4$, the vertices of the tetrahedra are repulsive, whereas the center of the face is attractive. In contrast, panel (b) corresponds to Fig. 3g (main text), and shows that removing the vertices of the tetrahedron has removed the repulsion, but the center of the face is still attractive. Panel (c) corresponds to Fig. 3k (main text) and shows (as does Fig. 3k) that the forces are less strong for cubes than the other two particles at this density. Moreover, it also shows that the cubic vertices are not acting repulsively at this density.

Entropic Torque In Monodisperse Hard Systems. In the main text we showed directional entropic forces between particles. Here we give an explicit calculation of the torque that aligns particles. As a simple example, consider a particle obtained from a sphere of radius r by cutting away the part of the sphere that intersects the half space $\mathbb{R}^3$ for which $z/r > \alpha$ to We performed MC simulations of systems of 1000 such particles with $\alpha = 0.01$ (nearly hemispherical) at fixed volume. Since the particles have axial symmetry, we their relative position and orientation can be characterized by four scalar quantities. If we take the separation between the particles to be $\vec{q}_{12}$, and their symmetry axes to be given by $\hat{n}_1$ and $\hat{n}_2$, then we are free to use

$$\Delta\xi_{12} = \{R \equiv |\vec{q}_{12}|, \phi_1 \equiv \hat{n}_1 \cdot \hat{q}_{12}, \phi_2 \equiv -\hat{n}_2 \cdot \hat{q}_{12}, \chi \equiv -\hat{n}_1 \cdot \hat{n}_2\} \quad [33]$$

In Table S1 we show the role of the PMFT in generating entropic torques that align particle facets in this system at a density of 50%. We find the potential difference between different particle orientations at fixed separation distance is of the order of a few $k_{\mathrm{B}}T$, giving rise to entropic torques strongly favouring alignment. Figures are height of the potential above the global minimum for slice of the potential with $\psi \equiv \phi_1 = \phi_2 = \chi$ fixed. Although the angular differences are small (perfect alignment is $\psi = 1$), the effective interaction varies by more than 2 k_BT over this angular range at small separations, indicating that the penalty for small misalignment is significant. Inset particle images illustrate the relative orientations shown.

Density Dependence. In Fig. 2 (main text) we showed that there was an effective attraction in the direction perpendicular to the particle face that increased as the density increased. We note here that this is not an effect of the increase in density alone. For example, in Fig. 2 we make a similar plot for cubes that, rather than passing through the potential minimum, passes through the vertex of one of the cubes. Comparing Fig. 2 with Fig. 2c (main text), we see that the effect of the particle shape leads to enhancement of face-to-face contact over and above what we would expect to observe based solely on the increase in density alone. This point is also underscored in Fig. 3 (main text) above.

[2] In practice, as described below we approximate each of these contributions by a $6N$ dimensional integral where six of the dimensions have a near-infinitesimal domain of integration.

Supplementary Discussion

Entropy. In this context, we should also comment further on the entropy that we are computing when we compute the PMFT. We have used the fact that, at least in principle, we can do statistical mechanics in any ensemble we find convenient. As usual, the entropy of the system is computed by counting all the microstates of the N particles in the system, and this can be obtained by performing (in the general case) the $6N$ dimensional integration over all of the positions and orientations of all particles. Here, for the purposes of isolating the effects of the particle shape, we have chosen to cast this integral as a series of $6(N-1)$ dimensional integrals, each of which describes the number of microstates available to the system when a particle pair is fixed to a certain relative position and orientation [2]. It is in the comparison of the relative entropic contributions from each of the integrals for pair configurations that we are able to identify the "microscopic" entropic origin of the "macroscopic" entropic ordering of the whole system seen in [3], and elsewhere in the literature. What is perhaps not intuitive about this process in the hard particle limit, which is like a microcanonical system in that all states have zero potential energy, is that this process entails splitting up the ensemble into configurations of fixed particle pair positions and orientations. We are, in effect, subdividing the microcanonical ensemble into yet smaller isobaric ensembles of states. Computations of this sort have appeared previously in the literature, see, *e.g.*, [4, 5].

Penetrable Hard Sphere Limit. Because the sea particles have repulsive interactions with the pair of interest, the pair behaves like part of the 'box' that constrains the sea. By moving the pair of interest we are changing the shape of the box from the point of view of the sea particles. The force exerted by the sea particles on the pair, then, is given by the stress tensor of the particles that are being integrated out on the boundary defined by steric hindrance with the pair of interest. We note, therefore, that the scale of this osmotic force is given by the scale of the stress tensor in the system; if the stress tensor is isotropic then this is just the pressure P, and so the scale of this force is given by $P\sigma^3/k_{\mathrm{B}}T$, where σ is a characteristic length scale.

In fact, the DEFs in monodisperse systems, defined above, are further strengthened by the addition of smaller soft depletants, as realized experimentally in [6, 7]. Typical colloidal experimental realizations of such systems require the depletants to induce interactions with strength between $\sim 4\ k_{\mathrm{B}}T$ (*e.g.* [8]) and $\sim 8\ k_{\mathrm{B}}T$ (*e.g.* [9]) to instigate binding. At very high depletant concentrations, estimates of the effective interaction strength can reach hundreds of $k_{\mathrm{B}}T$ (*e.g.* [8]). See [10] and references therein for more details on the experimental measurement of depletion forces.

Sea Particle Properties. We have shown in general that hard systems have an entropic preference for more densely packed pair configurations, because particle pairs are packed by the thermal motion of sea particles. The existence of correlations among the sea particles implies that the entropically preferred local dense packing for the pair is not generally the same as the global densest packing for the pair. However, if there are no correlations among the sea particles, their entropy depends *only* on the packing volume of the pair.

Intuitively, one can think of this as if the pair of interest is confined within some membrane under external pressure, provided by the boundary of the sea particles. If there is no correlation among the sea particles, the membrane will behave as if it has no internal stiffness, and will deform to squeeze the pair in any way they can be squeezed. However, if there are correlations among the sea particles, the membrane will act as if it has some inherent structure that prevents it from being deformed in any possible manner, and therefore the sea particles may not be able to pack the pair into *any* possible configuration.

Also, if one considers an initially monodisperse hard system, and takes the traditional (small) depletion limit at fixed system density, the number of sea particles will increase dramatically. To leading order the contribution from the sea particles scales like $-\beta N \log V$, which means that to preserve the packing density of the system, as we scale the characteristic size of the depletant σ, the sea particle contribution has scales (naively) as σ^{-3}. This means that systems of colloids and traditional, small, weakly interacting depletants, the osmotic pressure of the depletants can easily be much greater than the osmotic pressure of the other colloids, in determining the pair configuration. However, if the depletants are sufficiently large to be completely excluded from the region within a colloidal aggregate, then the shape entropy of the colloids within the aggregates then becomes important, as shown in an experiment by Rossi *et al.* [11].

Many-Body Interactions. The observation of face-to-face contacts in self-assembled systems, as noted in [12, 13], suggests that the effects of shape can be captured by an effective pair potential, such as the PMFT. Indeed we have shown in this paper a preference for polyhedra to align face-to-face, see Fig. 3 (main text). However, there are reported systems where coincident face-to-face alignment is not preferred, such as in octahedra (*e.g.* [12]). We regard these as many-body effects, which become more important at higher packing fractions, and which would be captured only by a many-body PMFT.

Formally, the n-body extension of the present techniques is straightforward; the only obstacle is to enumerate scalar invariant quantities for the n bodies, and compute their Jacobian. In practice, however, as n increases, so does the difficulty of obtaining sufficiently many measurements to compute the potential with accuracy.

Interaction Range. The range of DEFs is determined by the properties of the sea particles: their intrinsic interactions, size, shape, *etc.* Typically, we would expect that the sea particles generate an effective interaction between the colloids that is roughly of the order of the sea particle size. Given this intrinsic limitation, one might ask whether we can design shape features on the colloidal particles in order to control the assembly? This is developed in detail in [3]; we briefly comment on it here, too.

If the sea particles are small, noninteracting depletants, the range is sufficiently short that only shape features (on the colloidal pair) that are adjacent in closely packed configurations contribute to the interaction, *e.g.* flat faces in polyhedra, dimples and complementary spheres in lock-and-key experiments. [9, 14–16] Following [3], we identify these features as "entropic patches". Note that if the patches are sufficiently well-separated, the interactions are pair-wise additive, and so the effective potential energy of the colloids is given by the sum of the pair interaction energies.

If the sea particles are not small, or are interacting, then we would expect the interaction range to be longer, and the approximation that individual particle features can be considered separately as entropic patches may not always be valid, though we have preliminary results in several cases suggesting it still is. [17]

1. Ruszczyski, Andrzej. (2006) Nonlinear Optimization. (Princeton University Press, Princeton NJ).
2. Coumans, E. (2012) Bullet physics library (http://bulletphysics.org/). http://bulletphysics.org/.
3. van Anders, G, Ahmed, N. K, Smith, R, Engel, M, & Glotzer, S. C. (2014) Entropically patchy particles: Engineering valence through shape entropy. ACS Nano 8, 931–940.
4. Shieh, H.-H, van Anders, G, & Van Raamsdonk, M. (2007) Coarse-Graining the Lin-Maldacena Geometries. JHEP 0709, 059.
5. Balasubramanian, V, Czech, B, Larjo, K, Marolf, D, & Simon, J. (2007) Quantum geometry and gravitational entropy. JHEP 0712, 067.
6. Young, K. L, Jones, M. R, Zhang, J, Macfarlane, R. J, Esquivel-Sirvent, R, Nap, R. J, Wu, J, Schatz, G. C, Lee, B, & Mirkin, C. A. (2012) Assembly of reconfigurable one-dimensional colloidal superlattices due to a synergy of fundamental nanoscale forces. Proc. Natl. Acad. Sci. U.S.A. 109, 2240–2245.
7. Young, K. L, Personick, M. L, Engel, M, Damasceno, P. F, Barnaby, S. N, Bleher, R, Li, T, Glotzer, S. C, Lee, B, & Mirkin, C. A. (2013) A directional entropic force

approach to assemble anisotropic nanoparticles into superlattices. Angew. Chem., Int. Ed. 52, 13980–13984.
8. Mason, T. G. (2002) Osmotically driven shape-dependent colloidal separations. Phys. Rev. E 66, 060402.
9. Sacanna, S, Irvine, W. T. M, Chaikin, P. M, & Pine, D. (2010) Lock and key colloids. Nature 464, 575–578.
10. Lekkerkerker, H. N. W & Tuinier, R. (2011) Colloids and the Depletion Interaction. (Springer, Dordrecht).
11. Rossi, L, Sacanna, S, Irvine, W. T. M, Chaikin, P. M, Pine, D. J, & Philipse, A. P. (2011) Cubic crystals from cubic colloids. Soft Matter 7, 4139–4142.
12. Damasceno, P. F, Engel, M, & Glotzer, S. C. (2012) Crystalline assemblies and densest packings of a family of truncated tetrahedra and the role of directional entropic forces. ACS Nano 6, 609–614.
13. Damasceno, P. F, Engel, M, & Glotzer, S. C. (2012) Predictive self-assembly of polyhedra into complex structures. Science 337, 453–457.
14. Knig, P.-M, Roth, R, & Dietrich, S. (2008) Lock and key model system. Europhys. Lett. 84, 68006.
15. Odriozola, G, Jimenez-Angeles, F, & Lozada-Cassou, M. (2008) Entropy driven key-lock assembly. J. Chem. Phys. 129, 111101.
16. Odriozola, G & Lozada-Cassou, M. (2013) Statistical mechanics approach to lock-key supramolecular chemistry interactions. Phys. Rev. Lett. 110, 105701.
17. Ahmed, N. K, van Anders, G, Chen, E. R, & Glotzer, S. C. (2014). Submitted.